

## Anza palaeoichnological site, Late Cretaceous, Morocco. Part III: Comparison between traditional and photogrammetric records

Noura Lkebir<sup>a</sup>, Tanguy Rolland<sup>b</sup>, Fabrice Monna<sup>b,\*</sup>, Moussa Masrour<sup>a</sup>,  
Lhoussaine Bouchaou<sup>a,c</sup>, Emmanuel Fara<sup>d</sup>, Nicolas Navarro<sup>d,e</sup>, Josef Wilczek<sup>b,f</sup>,  
El Hassan Beraouz<sup>a</sup>, Carmela Chateau-Smith<sup>g</sup>, Félix Pérez-Lorente<sup>h</sup>

<sup>a</sup> Laboratory of Applied Geology and Geo-Environment, Ibn Zohr University, Agadir, Morocco

<sup>b</sup> ARTEHIS, UMR CNRS 6298, Université de Bourgogne-Franche Comté, 6 Boulevard Gabriel, bât Gabriel, 21000, Dijon, France

<sup>c</sup> International Water Research Institute (IWRI), University of Mohamed VI Polytechnic (UM6P), Benguerir, Morocco

<sup>d</sup> Biogéosciences, UMR CNRS 6282, Université Bourgogne Franche-Comté, 6 boulevard Gabriel, bât Gabriel, 21000, Dijon, France

<sup>e</sup> EPHE, PSL University, 75014, Paris, France

<sup>f</sup> Department of Archaeology, University of Hradec Králové, Rokytanského 62, 50003, Hradec Králové, Czech Republic

<sup>g</sup> CPTC, EA 4178, Université de Bourgogne, 4, boulevard Gabriel, 21000, Dijon, France

<sup>h</sup> Universidad de La Rioja, Edificio CT, Madre de Dios 51-53, 26006, Logroño, Spain

### ARTICLE INFO

#### Keywords:

Dinosaur  
Footprint  
Documentation  
Western high atlas  
Ichology  
Recording methods

### ABSTRACT

The present study evaluates a methodological workflow that could identify dinosaur tracks and trackways more comprehensively at outcrop scale. The approach described here is based both on 3D modelling by photogrammetry at different resolutions, and on suitably processed digital elevation models (DEMs). The ichnosite of Anza, Morocco, was chosen to demonstrate the efficiency of the proposed pipeline, because 323 dinosaur and pterosaur tracks discovered there have already been published. One subsector containing 89 tracks, identified in the two companion works that followed a traditional approach, was selected and divided into four subzones. By combining different DEM processes (hill-shade, slope, sky-view factor, and positive openness), almost twice as many tracks (175 vs 89) are now identified in these subzones. However, the improvement is not homogeneous. In the first subzone, the previous works reported 25 tracks vs. 22 with the 3D modelling techniques used here, whereas results for the second and third subzones show considerable improvement with 3D (21 vs 38 tracks and 42 vs 81 tracks, respectively). The enhancement is even more dramatic for the fourth subzone, where 34 new tracks are now identified, whereas with the traditional approach, only one track was previously reported. It is likely that such improvements depend on several factors, i.e. the surface conditions of the rocks (e.g. irregularities, cracking, etc.), and on the preservation state and depth of the tracks. Morphometric measurements of tracks and trackways obtained from 3D models are very similar to those derived from traditional fieldwork methods. The digital approach can be applied rapidly at different resolutions, but the models acquired with the pole-mounted camera provide a good compromise, with a resolution high enough (~2 mm/pix) to spot tracks, while respecting computational constraints. Once treated, DEMs greatly facilitate the reproduction of track outlines, drawn according to criteria defined by the operator.

### 1. Introduction

Since the seminal works of Hitchcock (1838, 1848, 1858), interest in dinosaur tracks and trackways has increased, especially in recent

decades. This is because tracks provide important information about both palaeobiology, including locomotion, behaviour, size, mass, and identity of trackmakers, and palaeoenvironment, including substrate physical properties, water saturation, and taphonomic features

\* Corresponding author.

E-mail addresses: [nouralkebir@gmail.com](mailto:nouralkebir@gmail.com) (N. Lkebir), [Tanguy.Rolland@u-bourgogne.fr](mailto:Tanguy.Rolland@u-bourgogne.fr) (T. Rolland), [Fabrice.Monna@u-bourgogne.fr](mailto:Fabrice.Monna@u-bourgogne.fr) (F. Monna), [moussamasrour5@gmail.com](mailto:moussamasrour5@gmail.com) (M. Masrour), [l.bouchaou@uiz.ac.ma](mailto:l.bouchaou@uiz.ac.ma) (L. Bouchaou), [emmanuel.fara@u-bourgogne.fr](mailto:emmanuel.fara@u-bourgogne.fr) (E. Fara), [nicolas.navarro@u-bourgogne.fr](mailto:nicolas.navarro@u-bourgogne.fr) (N. Navarro), [josef.wilczek@hotmail.com](mailto:josef.wilczek@hotmail.com) (J. Wilczek), [beraaouz@gmail.com](mailto:beraaouz@gmail.com) (E.H. Beraouz), [chateau.smith21@gmail.com](mailto:chateau.smith21@gmail.com) (C. Chateau-Smith), [felix.perez@ext.unirioja.es](mailto:felix.perez@ext.unirioja.es) (F. Pérez-Lorente).

<https://doi.org/10.1016/j.jafrearsci.2020.103985>

Received 28 April 2020; Received in revised form 1 July 2020; Accepted 18 August 2020

Available online 20 August 2020

1464-343X/© 2020 Elsevier Ltd. All rights reserved.

(Alexander, 1976; Gillette and Lockley, 1989; Lockley et al., 1986; Lockley, 1991; Thulborn, 1990; Lallensack et al., 2016; Falkingham et al., 2016; Pérez-Lorente, 2015). Dinosaurs have always fascinated the general public, and their tracksites are an indisputable asset for regional tourism (Laws and Scott, 2003; Monbaron and Monbaron, 2015; Alcalá et al., 2016; Cobos and Alcalá, 2017). Dinosaur tracksites can be found all over the world, except in Antarctica, where known tracks are extremely rare when compared with the known dinosaur fossil record (Gillette and Lockley, 1989; Olivero et al., 2007; Reguero et al., 2013). Documenting this rich palaeontological heritage worldwide is a challenging and time-consuming task. The most common ichnological method for studying dinosaur tracks (hereafter 'the traditional method') can be seen as a two-step process, involving track detection and measurement. For over a century, this process has generally been performed manually, in situ (Sarjeant, 1989; Thulborn, 1990; Falkingham et al., 2016; Gand et al., 2018). The first step is to mark tracks in the field with chalk (sometimes using a reference grid). The second step usually involves capturing and assembling pictures, vectorizing footprints, and measuring features of interest. In some instances, this step may also involve shading inside the imprints (e.g. highlighting some features, or tracing the track margin), or making an interpretative drawing on transparent paper. When tracks are barely visible, the use of oblique artificial light may be necessary at night, together with several field sessions for data verification or refinement. Typically, this acquisition process is slow, and requires a high level of expertise in the field, with several operators (Falkingham et al., 2016; Gand et al., 2018; Romilio et al., 2017). Over the last three decades, practical alternative or complementary solutions have emerged in ichnology, as considerable progress has been made in the field of 3D modelling and geometrical processing (Moratalla et al., 1988; Ishigaki and Fujisaki, 1989; Matthews and Breithaupt, 2001; Breithaupt et al., 2001, 2004; Matthews et al., 2005, 2006, 2016; Belvedere, 2008; Bates et al., 2008, 2009; Falkingham et al., 2009, 2016, 2018; Wings et al., 2016). Although lasergrammetry and scanners based on structured light were the first to be developed (Falkingham et al., 2016; Adams et al., 2010; Bates et al., 2010), they have not become common practice, due to heavy logistical constraints, and poor performance under direct sunlight (Falkingham et al., 2016; Matthews et al., 2016). In contrast, photogrammetry has become the near-standard approach in ichnology, sometimes associated with lasergrammetry, and more traditional approaches (Breithaupt et al., 2001; Breithaupt and Matthews, 2001; Adams and Breithaupt, 2003; Remondino et al., 2010; Mallison and Wings, 2014; Falkingham et al., 2016; Matthews et al., 2016; Mazin et al., 2016; Romilio et al., 2017; Moreau et al., 2020). Nonetheless, even though photogrammetry is now widely used to illustrate, selected representative tracks, it is only applied sporadically to represent entire sites. Orthomosaics and digital elevation models (DEMs) can be produced either by aerial or ground-based photogrammetry, at different resolutions (Kraus, 2007; Remondino et al., 2010; Falkingham, 2012; Falkingham and Gatesy, 2014; Matthews et al., 2016). Post-processing these DEMs may reveal features of special interest, such as peaks, valleys, ridges, and even anatomical details that would otherwise remain unnoticed in the field (e.g. for archaeological applications, see Magail et al., 2017; Monna et al., 2018). Several algorithms are available, based either on differential geometry (e.g. slope), or on visibility (e.g. sky-view factor, positive openness, and hill-shading). Each method reveals specific features of the relief, and their outputs can easily be integrated into geographical information systems (GIS), facilitating further measurements and spatial analysis (Matthews et al., 2016; Romilio et al., 2017). Although DEM acquisition by photogrammetry together with post-processing are commonly used to describe and document individual tracks and trackways, they have less frequently been combined with aerial imagery, despite the great potential of this approach (Breithaupt and Matthews, 2001; Matthews et al., 2016; Romilio et al., 2017).

The aims of the present study are (i) to propose a methodological workflow capable of identifying dinosaur tracks and trackways more

comprehensively, at outcrop scale, using 3D modelling at different resolutions, and (ii) to provide a quantitative comparison of the resulting outputs with those obtained by a more traditional approach. The workflow relies on images captured by Unmanned Aerial Vehicle (UAV), pole-mounted and hand-held cameras, creation of DEMs by Structure-from-Motion, and post-processing based on differential geometry and visibility. The Moroccan ichnosite of Anza, which is Coniacian-Santonian (Late Cretaceous) in age, is used as a case study. This large, multi-surface tracksite has already yielded 323 dinosaur and pterosaur tracks that have been investigated in companion works, using a traditional ichnological approach (Masrouf et al., 2017a,b). It is therefore an ideal candidate for comparisons between the traditional approach and 3D modelling, on the basis of their respective efficiency in spotting tracks, and of the similarity between field-derived and model-derived morphological measurements, both acquired by the same team of ichnologists. For the present study, 3D acquisition focused on a subzone of the Anza ichnosite (namely 1ANZ), where 89 dinosaur tracks have already been reported (Masrouf et al., 2017a,b). One of the main questions is to assess the level of 3D modelling resolution and the type of DEM post-processing necessary for specific ichnological analyses (e.g. ichnotaxonomical studies, and/or inventory and documentation of large tracksites).

## 2. Material and methods

### 2.1. Study site

The ichnosite of Anza is only briefly described here, as it has been extensively detailed in the two previous companion works (Masrouf et al., 2017a,b). It was discovered in 2013, about 5 km north of Agadir, Morocco, after an exceptional swell hit the Atlantic coast. The site consists of several calcareous sandstone beds, dating from the Coniacian-Santonian (Late Cretaceous), and is approximately  $100 \times 30 \text{ m}^2$  in extent. The area lies in the intertidal zone and is emergent for only a few hours a day. Except in winter, the site is often covered by a sand beach and/or by algae. These conditions considerably complicate the study of the site, but also provide natural protection against erosion. The entire area with mostly well-preserved dinosaur and pterosaur tracks has previously been divided into four geographical zones (i.e. 1ANZ, 2ANZ, 3ANZ, and 4ANZ in Masrouf et al., 2017a: Fig. 1). Two groups of vertebrate tracks have been clearly identified: theropod footprints, by far the most abundant (more than 300 tracks), and 11 pterosaur manus tracks found only in zone 2ANZ. At Anza, 56 trackways have previously been identified. Using quantitative morphometric features, Masrouf et al. (2017a,b) attributed the theropod tracks to *Grallator*-like or *Eubrontes*-like ichnogenera, and the pterosaur tracks to *Agadirichnus* or *Pterairchnus*. This ichnoassemblage, which also includes three tracks of the rare ichnogenus *Macropodosaurus*, makes Anza an international reference site for ichnology. When the photogrammetric campaign was undertaken, zones 2ANZ, 3ANZ, and 4ANZ were completely or partially covered by beach sand and algae. As it was not necessary to process the entire site to accomplish the aims of this study, only one subzone was targeted, zone 1ANZ, which is densely covered in theropod footprints (89 previously discovered tracks, over a surface area of ca.  $80 \times 10 \text{ m}^2$ ). Zone 1ANZ was almost free of sand or algae during photogrammetric acquisition, and exhibited surface rock conditions similar to those encountered during the previous (traditional) study, thus facilitating comparison.

### 2.2. Traditional approach for track documentation

Tracks at Anza were documented using the traditional method (Fig. 1). The first step was to draw the outline of all visible ichnites (i.e. the top of track walls at their intersection with the sediment surface) manually, with chalk, sometimes highlighting the limit of the extrusion rims and other remarkable features, such as pads and claw marks

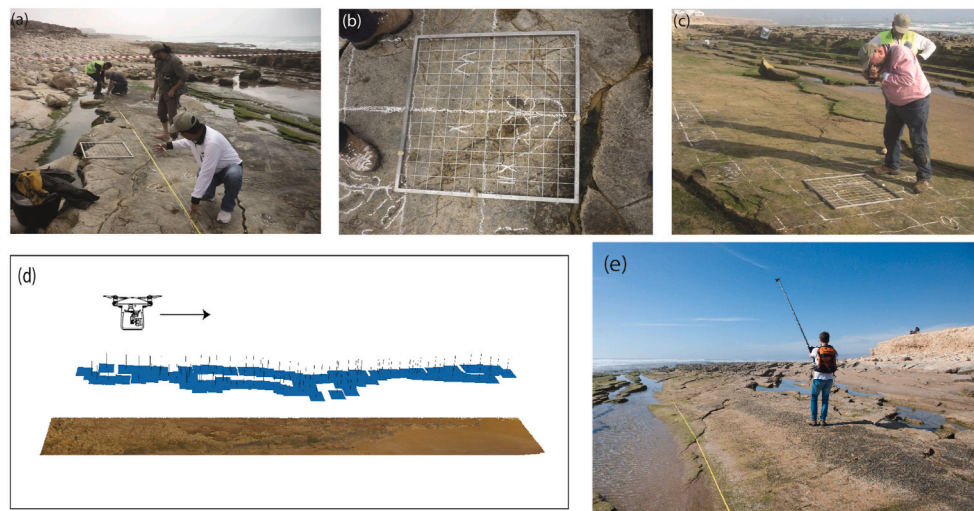


**Fig. 1.** Illustration of both traditional and 3D modelling methods. Traditional: (a) manual drawing of tracks with chalk, (b) grid drawing and alphanumeric referencing, (c) photographing tracks. 3D modelling: (d) flight of the UAV over the area of interest; blue rectangles correspond to images captured, (e) images captured by pole-mounted camera. (For interpretation of the references to colour in this figure legend, the reader is referred to the Web version of this article.)

(Fig. 1a). A series of  $30 \times 30 \text{ cm}^2$  squares (Fig. 1b) was also drawn on the track-bearing surface, forming a grid with axes corresponding to the dip and strike lines of the surface (Masrou et al., 2017a,b). Each cell of this grid was referenced using an alphanumeric system, and then photographed as perpendicularly as possible to the bed surface, to obtain views with minimal distortion due to perspective (Fig. 1c). In the laboratory, the photographs were first rectified to eliminate any remaining perspective distortion. They were then assembled with Adobe Photoshop®, a raster graphics editor, to produce a document in a projection plane parallel to the rock surface where the tracks lie. Once scaled and referenced in a metric system, the final photo-assemblage was transferred into Autodesk AutoCAD®, a computer-aided design software, to vectorize the tracks, and to measure a set of morphometric features, including distances, angles, and derived variables (Fig. 2). It is worth mentioning that these measurements were in good agreement with those taken in the field for some selected tracks.

### 2.3. Photogrammetric workflow

Whatever the size of the objects studied, and the desired DEM resolution, 3D modelling was obtained by Structure-from-Motion. This technique is increasingly used in several scientific fields, e.g. geology and geomorphology (Bemis et al., 2014; Tavani et al., 2016; Westoby et al., 2012), and archaeology and cultural heritage (López et al., 2016; Monna et al., 2018; Reu et al., 2013; Verhoeven et al., 2012). Briefly, a set of pictures covering the area of interest is captured, while (i) maintaining an overlap between pictures of at least 70–80%, and (ii)

changing the point of view between each shot. For nearly flat surfaces, as in our case, the pictures are taken in the nadir direction, as perpendicularly as possible to the surface, to reduce image distortion. A 3D reconstruction is obtained after estimating camera positions and orientations, producing a sparse cloud, densifying this cloud, then meshing, and texturing. The resulting images (i.e. 2.5D grids) are saved in raster format. Note that the resolution of a DEM depends on the size and resolution of the camera sensor, the focal length of the lens, and the distance between the camera and the outcrop. Here, four different resolutions were evaluated. First, the entire site was modelled with the help of the UAV, a DJI Phantom 3 PRO equipped with a GPS and a 12-million-pixel camera (Fig. 1d, Table 1). The flight height of ca. 15 m led to a ground sample distance or GSD (i.e., the distance between the centres of two consecutive pixels) of about 5–6 mm. The result was a georeferenced orthomosaic and DEM covering the whole area. Next, to better define altitudinal surface variation, pictures were also captured at a lower elevation, using a SONY DSC-RX100 MIII (sensor  $13.2 \times 8.8 \text{ mm}^2$ , 20 Mpix), with a 24–70 mm lens, equivalent to a full-frame 35 mm camera set at 24 mm. The camera was mounted on a 4-m-long telescopic Rode pole, and wifi-controlled, using a Samsung Galaxy tablet fixed to the pole (Fig. 1e). A total of 9 slightly overlapping chunks was produced, each about  $100 \text{ m}^2$ , with a typical GSD of 1–2 mm (Table 1). The other two acquisitions were made with a hand-held NIKON D800 full-frame DSLR (sensor  $24 \times 36 \text{ mm}^2$ , 36 Mpix), equipped with a NIKKOR 50 mm prime lens. Three small areas of about  $10\text{--}20 \text{ m}^2$ , each containing a set of footprints, were selected and photographed at breast height (1.5–1.6 m from the ground), delivering DEMs with a GSD of about

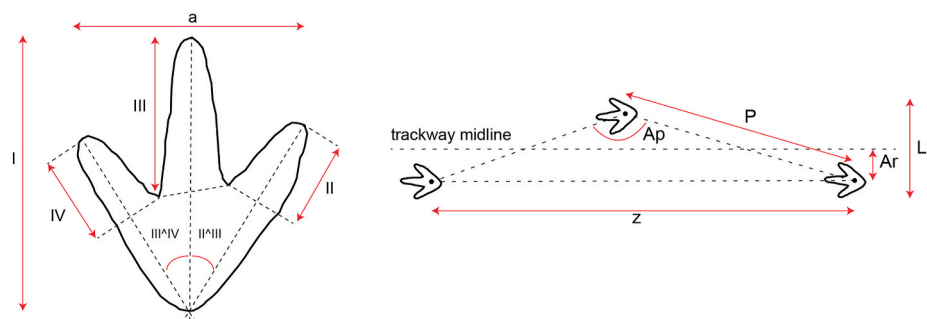


**Fig. 2.** Ichnological parameters measured in Masrou et al. (2017b) and in the present study. *l*: footprint length; *a*: footprint width; *Ar*: trackway deviation; *Lr*: trackway external width; *P*: pace length; *z*: stride length, *Ap*: pace angle; *II*<sup>^</sup>*III*<sup>^</sup>*IV*: lengths of digit impressions; *II*<sup>^</sup>*III*<sup>^</sup>*IV*: interdigital angles.

**Table 1**

Acquisition settings. Type of view, object targeted, ground distance, camera type, sensor definition, number of pictures processed, focal length of the lens (\*: equivalent on full frame, 35 mm camera) and typical resolution of the produced DEMs.

| Type of view  | Object targeted      | Ground distance | Camera type       | Definition | Number of pictures processed                | Focal length of the lens | Typical resolution of produced DEM |
|---------------|----------------------|-----------------|-------------------|------------|---|--------------------------|------------------------------------|
| Aerial        | Entire site          | ~15 m           | DJI Phantom 3 PRO | 12 Mpix    | ~100 for 1000 m <sup>2</sup>                | 20 mm*                   | 5–6 mm/pix                         |
| Pole          | Bed                  | ~4 m            | SONY RX-100MIII   | 20 Mpix    | ~50 per chunk of ca. 50 m <sup>2</sup>      | 24 mm*                   | 1–2 mm/pix                         |
| Breast height | Trackways/footprints | 1.5–1.6 m       | Nikon D800        | 36 Mpix    | ~100–150 per chunk of ca. 20 m <sup>2</sup> | 50 mm                    | 100–150 μm/pix                     |
| Close up      | Footprints           | 0.4–0.6 m       | Nikon D800        | 36 Mpix    | 10–20 per footprint                         | 50 mm                    | 50–80 μm/pix                       |

100–150 μm. For individual footprints, the best DEM resolution was obtained by capturing images with the operator crouching at 0.5–0.6 m above ground level, generating DEMs with a GSD of ca. 50–80 μm. Only one isolated footprint, 1.3ANZ9, and 15 footprints from trackway 1.3ANZ5 (Masrouer et al., 2017b) were acquired at this level of precision. Models produced by terrestrial photogrammetry, generated in an arbitrary reference system, were aligned on the georeferenced UAV orthomosaic, using several ground control points. All georeferenced DEMs and orthomosaics were then integrated into GIS software, for further measurement.

2.4. Algorithms used to treat DEMs

Geomorphologists have developed several algorithms to identify geomorphological features (depressions, slopes, etc.) at the scale of a landscape, which can be used to reveal footprints. Slope describes the maximum rate of change in elevation between each cell of the raster and its neighbours. This is the maximum downhill gradient, calculated as the first derivative of the DEM (e.g. Longley, 2005). The most basic procedure based on visibility is analytical hill-shading, which simulates artificial illumination of the DEM surface (Imhof, 2007). The idea underlying the sky-view factor is that the bottom of a depression receives less light than the summit of a peak. Sky-view factor (SVF) evaluates that part of the hemispheric sky limited by the relief, and visible from a given point within a searched radius, *r* (Fig. 3a). In practice, *n* directions (most often 8) are scanned, and the vertical angles starting from the horizon to the position where the sky becomes visible,  $\gamma_i$ , are assessed; SVF is then

computed as follows (Zaksek et al., 2011):

$$SVF = 1 - \frac{\sum_{i=1}^n \sin \gamma_i}{n}$$

The same principle governs the calculation of positive openness, reflecting the “degree of dominance or enclosure of a location on an irregular surface” (Yokoyama et al., 2002; Doneus, 2013). The main difference is that the greatest angle before interception with the surface,  $\alpha$ , is sought, taking the zenith as reference in place of the horizon, in contrast with sky-view factor (Fig. 3b). Consequently, a constant slope is seen as a flat surface by positive openness, whereas the summit of a peak produces the same result as a horizontal plane with sky-view factor (Fig. 3c). Practically, 8 directions (N, NW, W, SW, S, SE, E, and NE) are evaluated at each point of the DEM, and positive openness,  $\alpha_{PO}$ , is obtained by simply averaging:

$$\alpha_{PO} = \frac{(\alpha^0 + \alpha^{45} + \dots + \alpha^{315})}{8}$$

2.5. Software and hardware

All DEMs were produced using the Agisoft Photoscan Pro software 1.4.5. The hill-shading, slope, and visibility-based rasters were created with either the open-source QGIS (<https://www.qgis.org>) or SAGA GIS (<http://www.saga-gis.org/>) software. Traditional morphometric measurements were obtained in QGIS from tracks drawn as vector layers. Unreferenced schemes from the companion studies (Masrouer et al.,

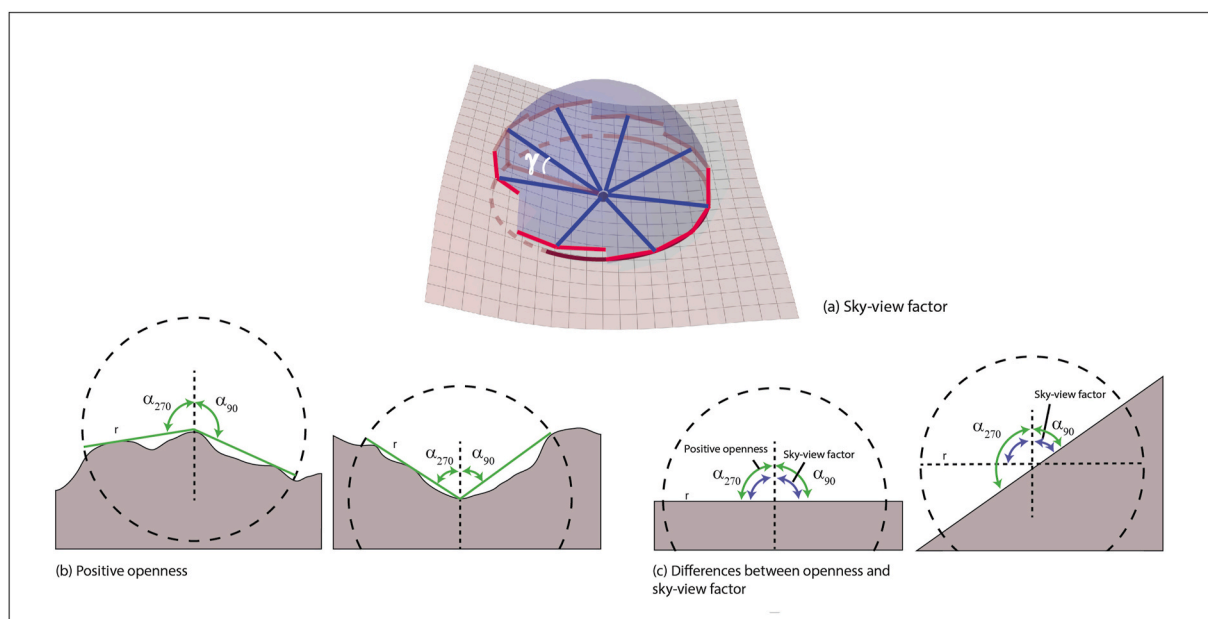


**Fig. 3.** Principles of (a) sky-view factor, and (b) positive openness; drawing modified from Dozier and Frew (1990) and Monna et al. (2018). The differences between both the two parameters are illustrated in (c).

2017a,b) were registered using a rigid Helmert transformation, selecting several control points on trackways. A consumer-grade computer, i7 5960x, 8 cores, equipped with 64 Go of RAM and two 4 Go-RAM NVIDIA GeForce GTX 980 mounted in SLI, was used for processing.

### 3. Results and discussion

#### 3.1. Track identification from processed DEMs

Identifying and understanding the factors that have preserved dinosaur footprint morphology is a complex task. The track preservation state results from many factors, such as the nature of the substrate, the depth of the footprint, the effect of erosional processes, and the possible presence of extra-morphological structures. Orthomosaics, DEMs, and derivatives, at all available resolutions, were used to evaluate the intrinsic potential of 3D modelling for track detection and drawing, without reference to field data or previously published schemes. When optimal foot dynamics and substrate properties record the anatomy of the foot, depressions caused by a moving dinosaur should be characterized by low sky visibility (i.e. low values of sky-view factor and positive openness), surrounded by subvertical footprint walls (i.e. steeply sloped contours). Even when tracks have been identified, drawing individual tracks sufficiently well is always a challenge, as there is often room for debate on where the track contours should be drawn (Graversen et al., 2007; Milàn and Loope, 2007; Falkingham, 2016; Lallensack et al., 2016). Following many authors (e.g. Ishigaki and Fujisaki, 1989; Lallensack et al., 2016), and similarly to the previous companion works, the outline of the track wall is preferred here (i.e. at the top of the track wall) to allow quantitative comparison. Fig. 4 depicts orthomosaic, DEM, hill-shaded DEM, slope, sky-view factor, and positive openness raster maps of footprint 1.3ANZ9, together with the values for each parameter, along an A-B profile crossing the footprint. This example, based on a well-preserved footprint, presents acquisition at the highest resolution ('close-up' in Table 1). The guidelines mentioned below are valid whatever the resolution. Here, the outline is barely visible on the orthomosaic, blurred by texture variation due to erosion and algae (Fig. 4a). From the DEM, incisions made by digits become unambiguous; the talwegs (Fig. 4b, n°1 and n°3) can be positioned precisely, as well as the ridge (Fig. 4b, n°2), but it is still difficult to delineate the footprint with precision without DEM post-processing. Hill-shaded raster is effective for quickly perceiving the relief, which is rendered realistically (Fig. 4c). However, there are major differences in the depiction of slopes in terms of brightness, depending on their orientation relative to artificial light (from the northwest in this case). The steepness of slopes is poorly rendered. Ridges and talwegs are displayed in mid-grey. The rear wall of the footprint, parallel to the light beam (Fig. 4c, n°4), is not clearly distinguished because of its orientation. Slope raster can be used to alleviate the above-mentioned drawbacks. The footprint is easily visible, marked by steep slopes (darker colour in Fig. 4d). Its outline is characterized by a sharp decrease in slope, which can also be observed for talwegs. To compute sky-view factor and positive openness, the maximum search radius needs to be tuned, which is not the case for hill-shading and slope (Fig. 4e and f). Search radius, an important parameter, must be set by taking into account the size of the features to be highlighted: higher values enhance the main structures, while details are better depicted when the radius decreases. As a rule of thumb, if the entire depression must be darkened, the search radius must be at least half the diameter of the object (Mara et al., 2010; Zaksek et al., 2011). The 1.3ANZ9 footprint measures approximately  $20 \times 20 \text{ cm}^2$ , and a search radius greater than 10 cm would be a good first guess. However, with such a value, most of the details inside the footprint would disappear, which is why a smaller radius (5 cm) was used here. With both sky-view factor and positive openness (Fig. 4e and f), contrasts with steep slopes within the track are well marked in dark tones, and may ultimately help to delineate the outline, while the "heel" is identified by a small (darker) hollow within

the larger depression formed by the entire footprint. Imprints of digits II and III are extremely dark because the corresponding impressions are very deep and narrow. At first glance, the drawings based on each individual treatment appear quite similar (see blue contours in Fig. 4c–f, and Fig. 4g, where all contours are superimposed). However, some notable differences can be observed. Using hill-shading, a gap without any clear information had to be filled in at the bottom left outer limit of the footprint (dashed line in Fig. 4d). The identification of this limit is easier with the slope raster, as well as with the sky-view factor and positive openness. However, both the slope and the hill-shaded rasters suggest some sinuosity in the imprint of digit III (Fig. 4c–d, n° 5), which cannot be perceived with the other two processes. Sky-view factor and positive openness produce similar outputs, except that positive openness slightly outperforms sky-view factor in detecting hypices (Fig. 4e–f, n°6). It is well known that defining the contours of dinosaur tracks is somewhat subjective (Thulborn, 1990; Bates et al., 2008; Romilio and Salisbury, 2014; Falkingham, 2016; Falkingham et al., 2018), and can challenge the operator during the drawing phase. The best solution here is probably the detailed examination of every raster map, including the orthomosaic. The definitive outline is then produced by following an interpretative process, which takes advantage of the features of interest provided by each treatment (Fig. 4h). A return to the field may, however, be worthwhile to refine the final drawing of the tracks.

#### 3.2. Mapping and track census

Except for the deepest tracks (depth > 2 cm, as for 1.3ANZ9), the resolution obtained here from aerial photography by UAV (~5–6 mm for x and y, 1 cm for z) is not good enough to perceive dinosaur footprints (see the slope raster map for track 1.3ANZ5.13, Fig. 5). Its usefulness is mainly limited to georeferencing the other layers, and also obtaining an overall image of the study area. In contrast, the outputs obtained from images taken at breast height or crouching are extremely well defined (Fig. 5). Although the resolution for images captured when crouching is about twice that of those taken at breast height, no significant discrepancy is observed. Unfortunately, high-resolution acquisition was limited here to a few specific areas, because covering the entire Anza ichnosite would require too much computation power for the hardware available for this study. This is one of the drawbacks of the 3D approach, in comparison with traditional methods. Identification and drawings were therefore essentially based on the models acquired with the pole-mounted camera (resolution ~2 mm/pix, Fig. 5), which provide a good compromise, with resolution high enough to spot tracks, while respecting computational constraints. In cases where some doubt persists, it is still possible to inspect other available raster maps obtained at higher resolutions, because GIS allows a seamless switch across layers. As the study area is elongated, it was divided into four zones (red rectangles in Fig. 6), with the same designation as in Masrou et al. (2017b) for the first three zones (1.1ANZ, 1.2ANZ, and 1.3ANZ), and a fourth zone (1.4ANZ), created specifically for the present study. In total, 175 easily distinguishable footprints were recorded, without any input from the previous companion works (Masrou et al., 2017a,b), which identified 89 tracks using the traditional approach (Fig. 7). However, this increase in the number of tracks is not homogeneous across the four zones in Anza 1. The traditional approach revealed 25 tracks vs. 22 with 3D modelling techniques in zone 1.1ANZ (Fig. 7). The 3D approach outclasses the previous study by a factor of almost two, for zones 1.2ANZ (21 vs 38 tracks) and 1.3ANZ (42 vs 81 tracks). This discrepancy is even more pronounced for zone 1.4ANZ, where 34 new footprints are now identified, while only one track was reported with the traditional approach (Fig. 7). In zone 1.1ANZ, the lower rate of identification using raster maps is probably due to strong surface irregularities and erosion/cracking. Such irregular surfaces impede the unambiguous recognition of footprints from post-processed DEMs. In this case, careful inspection in the field clearly outperforms 3D modelling and associated processing methods. For well-marked footprints, visible even to a

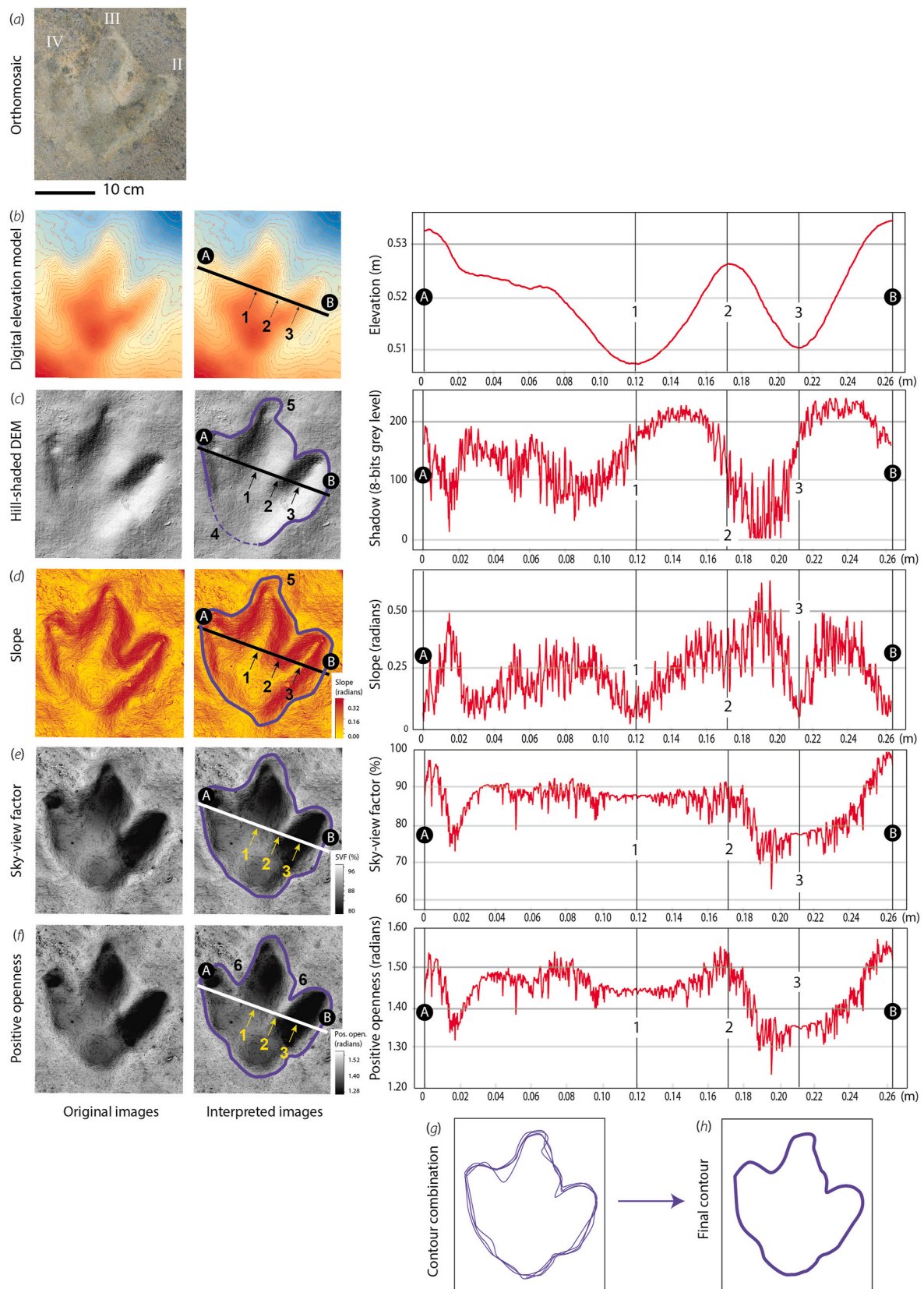


**Fig. 4.** Algorithm tests on footprint 1.3ANZ9 track, approximately  $20 \times 20 \text{ cm}^2$  wide. (a) orthomosaic; (b) coloured DEM and contour lines (2 mm interval); (c) hill-shaded DEM; (d) slope; (e) sky-view factor; (f) positive openness; (g) combination of contours obtained from each DEM treatment; (h) final interpretative contour. Sky-view factor and positive openness were computed with a radius of 5 cm. On the left-hand side, the original raster maps, and their interpretation; on the right-hand side, values along an A-B profile across the footprint. Numbers refer to special points of interest (see text for details).

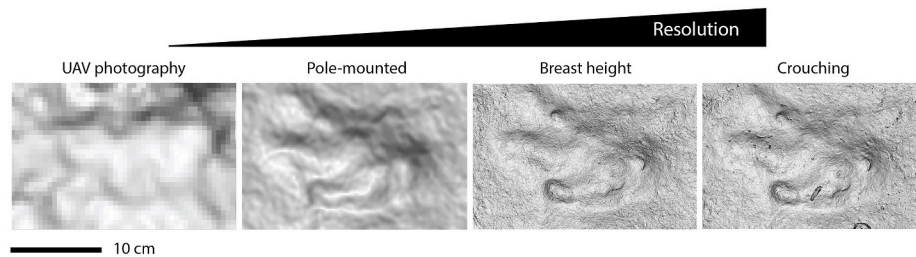


Fig. 5. Typical rendering of a footprint (1.3ANZ5.13) at the four resolutions evaluated. Resolution increases from left to right.

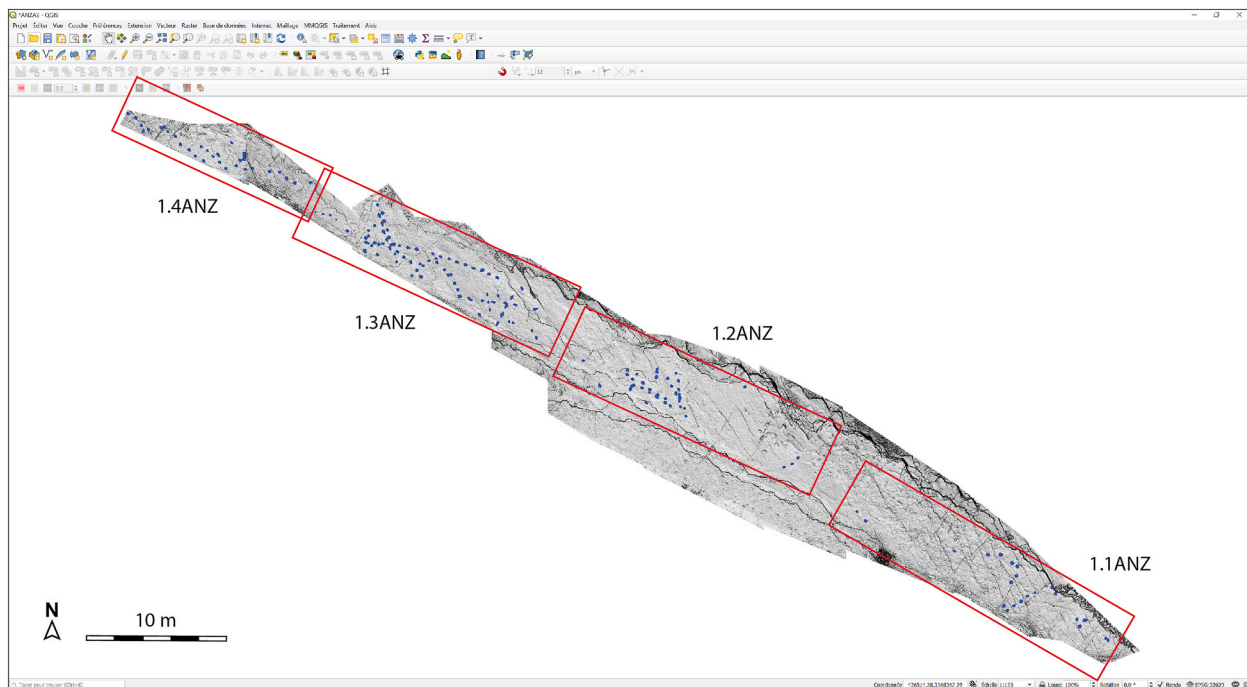


Fig. 6. Processed raster maps of the Anza ichnosite in a geographical information system (QGIS). Zone 1ANZ processed with hill-shading. The study area is divided into four subzones, following the denominations in Masrou et al. (2017b) for zones 1.1ANZ, 1.2ANZ, 1.3ANZ, together with the newly created zone 1.4ANZ. Drawings of dinosaur tracks identified in this study appear as an overlying shapefile in blue. (For interpretation of the references to colour in this figure legend, the reader is referred to the Web version of this article.)

non-specialist, the two approaches provide the same results. By contrast, post-processed DEMs reveal very small variations in elevation that would have not be visible in the field without special equipment, e.g. artificial light by night. This level of definition, and the possibility of visualizing a trackway in its entirety, together explain why raster maps efficiently complement the traditional method, essentially based on field work. Finally, positioning tracks by 3D modelling is likely to be more accurate, because the necessary movements of the palaeontologist in the field, even when proceeding cautiously, will almost always produce outputs somewhat undermined by the cumulative effect of small positioning errors.

The time factor is also worth mentioning. Only half a day was necessary for one operator to acquire photographs at the four resolutions used here, with a further ten days for DEM production and post-processing. Interestingly, this pipeline requires very little supervision by the operator. This time frame should be evaluated in comparison with several weeks of work at best, requiring the presence of two (or more) palaeontologists, where progress may well be impeded by external factors, such as the recurrence of the tide, as in the case of the Anza ichnosite. The only potential drawback is that producing a photogrammetry-based ichnological record is still computer-intensive at the time of writing.

### 3.3. Morphometric measurements

Another aim of this work was to evaluate the efficiency of raster maps in producing accurate morphometric measurements. As no true reference values exist, the results obtained from 3D models can only be compared to the data published in Masrou et al. (2017b). Derived variables obtained from two (or more) measurements are discarded; only primary variables are kept: footprint length, footprint width, trackway deviation (distance between footprint midpoint and trackway midline), trackway external width, pace length, stride length, pace angle, footprint orientation (angle between footprint axis and midline of trackway), length of digit impressions, interdigital angle, and trackway direction. Results for the two approaches are summarized in Table 2. They are reported as averages of distances and angles of footprints and trackway for the traditional approach. For the 3D method, they are given as a range of values when  $n < 4$ , and as a mean with its 95% confidence interval in all other cases. At the Anza ichnosite, there is overall agreement between measurements for the two approaches, and cases of mismatch are rare (in bold in Table 2), with divergence at only 10–15%. Such convergence may also be the result of the greater number of footprints discovered through 3D modelling. The pertinence of the results obtained by the two approaches nevertheless remains dependent

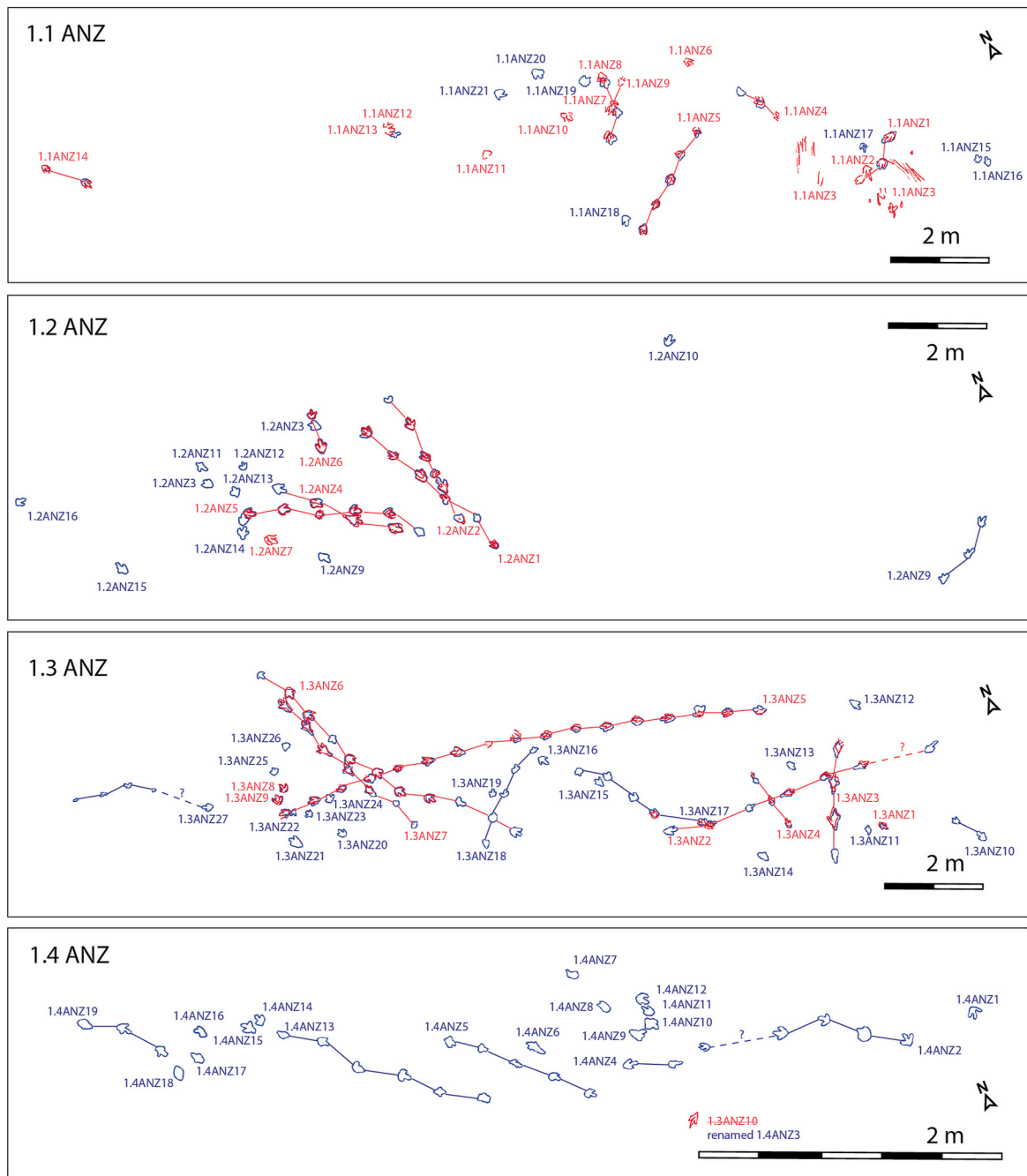


**Fig. 7.** All dinosaur tracks, showing those from Masrou et al. (2017b) in red, and those identified in the present study using medium resolution (pole-mounted camera) in blue. Names of tracks/trackways follow the denominations in Masrou et al. (2017b). Note that footprint 1.3ANZ10, which originally belonged to the 1.3ANZ subzone, was renamed 1.4ANZ3 to fit the creation of a new subzone (1.4ANZ). (For interpretation of the references to colour in this figure legend, the reader is referred to the Web version of this article.)

on the choices made by palaeontologists with regard to what should be measured.

#### 4. Concluding remarks

The results obtained from the Anza ichnosite show that the proposed protocol may outperform the traditional method in some instances, in terms of the number of footprints discovered (here the number of footprints identified is increased by a factor of two), and probably also in terms of the information necessary for contour drawings. Such great improvement in terms of track identification is obviously not expected for all sites, especially for those with well-preserved tracks, where both

methods should produce very similar results. It is important to note that many of the new discoveries in this study concerned poorly preserved, vanishing, shallow tracks, with barely defined walls, identified without ambiguity by the 3D approach. An additional pterosaur track was also detected in zone 2ANZ (not shown here) by means of this methodological workflow. The greatest benefit of this method is undoubtedly the small amount of time spent in the field. Field study is probably the most limiting factor for massive acquisition, especially for sites at some distance from the laboratory, which are often time-constrained, and where repeated access on demand may be difficult, due to cost, schedules, seasonal constraints, etc.

The optimal methodological pipeline may consist first in screening



**Table 2**

Measurements in centimetres from Masrou et al. (2017b), referred to as the traditional method (Trad. meth.) and measurements derived from the 3D models of the present study. Abbreviations: *n*: number of footprints taken into account in the calculation; *l*: footprint length; *a*: footprint width; *Ar*: trackway deviation; *Lr*: trackway external width; *P*: pace length; *z*: stride length, *Ap*: pace angle; *O*: footprint orientation; II-III-IV: lengths; II<sup>^</sup>III<sup>^</sup>IV: interdigital angles; *N-E*: trackway direction (e.g. N243). For the traditional method, the values correspond to measurement averages. For the 3D-derived measurements, the values are provided as range, when *n* < 4, and as mean with its 95% confidence interval, otherwise. Cases where the 3D approach does not match the traditional method are noted in bold. NA for Not Available.

| Trackways |             | <i>n</i> | <i>l</i>      | <i>A</i>     | <i>Ar</i> | <i>Lr</i> | <i>P</i>     | <i>z</i>       | <i>Ap</i>      | <i>O</i> | II-III-IV    | II <sup>^</sup> III <sup>^</sup> IV | N ... E |
|-----------|-------------|----------|---------------|--------------|-----------|-----------|--------------|----------------|----------------|----------|--------------|-------------------------------------|---------|
| 1.1ANZ1   | Trad. meth. | 3        |               | 18           | 8         | 36        | 58           | 113            | 160            |          |              | 13-31                               | 243     |
|           | 3D          | 2        |               | 17-18        | 7         | NA        | 62           | NA             | NA             |          |              | 17-30                               | 242     |
| 1.1ANZ5   | Trad. meth. | 5        | 23            | 17           | 1         | 23        | 59           | 119            | 172            | 0        |              | 25-30                               | 237     |
|           | 3D          | 5        | 22 ± 4        | 16 ± 3       | 1         | 26        | 57-62        | 116-121        | 168-173        | 0        |              | 27-34                               | 243     |
| 1.1ANZ8   | Trad. meth. | 3        | <b>23</b>     | <b>21</b>    | 7         | 34        | 63           | 123            | 153            |          | 12-15 - 19   | 23-42                               | 203     |
|           | 3D          | 2        | <b>24-25</b>  | <b>24-26</b> | 8         | NA        | 71           | NA             | NA             |          | 11 - 15 - 16 | 29-44                               | 207     |
| 1.1ANZ14  | Trad. meth. | 2        | <b>22</b>     | 18           |           |           | 93           |                |                |          |              |                                     | 140     |
|           | 3D          | 2        | <b>24-26</b>  | 13-19        |           |           | 94           |                |                |          |              |                                     | 147     |
| 1.2ANZ1   | Trad. meth. | 5        | 18            |              | 2         | 23        | 60           | <b>120</b>     | 171            | -4       | 14           | 19-26                               | 337     |
|           | 3D          | 6        | 21 ± 4        |              | 2         | 26        | 62 ± 6       | <b>122-123</b> | 163-174        | -5       | 13-00 - 00   | 20-26                               | 330     |
| 1.2ANZ2   | Trad. meth. | 4        | 23            | 18           | 2         | 19        | 62           | 123            | <b>172</b>     | 7        | 09 - 13 - 16 | 36-36                               | 356     |
|           | 3D          | 5        | 24 ± 4        | 18 ± 3       | 3         | 25        | 58-70        | 122-127        | <b>163-171</b> | 8        | 10-14 - 15   | 34-36                               | 362     |
| 1.2ANZ4   | Trad. meth. | 3        | 25            | 20           | 4         |           | <b>77</b>    | <b>154</b>     | 170            |          |              |                                     | 131     |
|           | 3D          | 4        | 24-28         | 19-25        | 4         |           | <b>62-72</b> | <b>132-142</b> | 170-174        |          |              |                                     | 129     |
| 1.2ANZ5   | Trad. meth. | 5        | 20            | 18           | 3         | 25        | 62           | 123            | 170            | -1       | 10-13 - 16   | 30-35                               | 114     |
|           | 3D          | 5        | 27 ± 11       | 21 ± 3       | 2         | 26        | 66 ± 22      | 116-133        | 162-174        | 0        | 9 - 12 - 17  | 32-35                               | 120     |
| 1.2ANZ6   | Trad. meth. | 2        | 23            | 19           |           |           | 51           |                |                |          |              | 21-31                               | 353     |
|           | 3D          | 2        | 22-27         | 18-21        |           |           | 63           |                |                |          |              | 22-31                               | 360     |
| 1.3ANZ2   | Trad. meth. | 3        |               | 14           | 1         | 18        | 80           | 160            | 175            |          |              |                                     | 98      |
|           | 3D          | 6        |               | 15 ± 2       | 0         | 20        | 84 ± 9       | 167 ± 15       | 168-177        |          |              |                                     | 100     |
| 1.3ANZ4   | Trad. meth. | 3        | 15            | 10           | 0         | 11        | 57           | 115            | 180            | 0        |              |                                     | 354     |
|           | 3D          | 3        | 20-23         | 14-16        | 1         | 12        | 54-60        | 115            | 175            | 0        |              |                                     | 350     |
| 1.3ANZ5   | Trad. meth. | 17       | <b>20</b>     | 13           | 1         | 16        | 62           | 124            | 175            | 0        | 09 - 13 - 15 | 25-23                               | 267     |
|           | 3D          | 16       | <b>25 ± 1</b> | 15 ± 2       | 1         | 15        | 6 ± 2        | 125 ± 2        | 175 ± 1        | 1        | 10-14 - 15   | 25-24                               | 261     |
| 1.3ANZ6   | Trad. meth. | 6        | 24            | 20           | 5         | 23        | 60           | 119            | 165            | -5       |              | 12-30                               | 156     |
|           | 3D          | 8        | 28 ± 2        | 18 ± 2       | 5         | 25        | 62 ± 3       | 123 ± 4        | 162 ± 12       | -4       |              | 14-33                               | 155     |
| 1.3ANZ7   | Trad. meth. | 5        |               | 21           | 4         | 31        | 61           | 122            | 170            | -2       |              | 30-40                               | 344     |
|           | 3D          | 7        |               | 21 ± 1       | 4         | 33        | 60 ± 5       | 117 ± 5        | 165 ± 11       | -1       |              | 32-39                               | 340     |

the area of interest using the UAV, to obtain a georeferenced orthomosaic, to which will be attached the other models (even simple photographs), at higher resolution. An even better solution would be to use an available UAV equipped with a high-quality camera sensor, at lower altitude, thus replacing the acquisition steps using a pole. Whether derived from UAV or pole images, 3D models with resolution from about 1 to 2 mm lead to good recognition of tracks (at least here), in particular because entire trackways can be depicted on raster map outputs. At the current level of technical and computational constraints, it may be difficult to produce models over large areas, at resolution better than 100 µm per pixel. This resolution is nevertheless adequate when assessing rock surface condition (e.g. the effect of bioturbation and erosion), and for determining and interpreting ichnotaxa. While awaiting further technical improvements and better calculation power, such high-resolution models should probably be limited to smaller areas, studied for specific purposes, or for verification, after preliminary screening at a lower resolution. In any case, a return to the field is strongly recommended to confirm and refine the results obtained computationally. Even if the documentation thus produced is probably more reliable and less operator-dependent than the traditional method, the identification and the interpretative drawings made by the operator still require a high level of expertise, as several choices must be made. Interestingly, the production of several maps derived from the DEM (hill-shaded DEM, slope, sky-view factor, and positive openness) should help palaeontologists to draw track outlines, in accordance with the criteria used for defining track contours. The workflow described here, using an appropriate UAV, may be applied safely to hard-to-reach ichnological sites, such as those found on strongly tilted (or even vertical) surfaces. Finally, for rapidly eroding sites such as Anza, these methods allow the operators to record quickly and efficiently a large number of potentially vulnerable tracks, which is complicated logistically with traditional casting methods. The 3D documentation may also serve to assess the impact of erosion dynamics on the morphology of fossil tracks. This method complements manual drawing, making tridimensional

geometry available for future scientific research, 3D printing, virtual reality, presentation in museums, and other techniques of digital scientific outreach via the web.

#### Declaration of competing interest

The authors declare that they have no known competing financial interests or personal relationships that could have appeared to influence the work reported in this paper.

#### Acknowledgements

We are grateful to Martin G. Lockley, an anonymous reviewer, and the associate editor for their constructive comments, which have greatly improved the manuscript.

#### Appendix A. Supplementary data

Supplementary data to this article can be found online at <https://doi.org/10.1016/j.jafrearsci.2020.103985>.

#### References

- Adams, T.L., Strganac, C., Polcyn, M.J., Jacobs, L.L., 2010. High resolution three-dimensional laser scanning of the type specimen of *Eubrontes(?) glenrosensis* Shuler, 1935, from the Comanchean (Lower Cretaceous) of Texas: implications for digital archiving and preservation. *Palaeontol. Electron.* 13 (3), 11p.
- Adams, T.C., Breithaupt, B.H., 2003. Mid jurassic dinosaurs of northern Wyoming: evidence from yellow brick road dinosaur tracksite, bighorn basin, Wyoming. *Wyoming Geo Notes* 78, 39-46.
- Alexander, R.M.N., 1976. Estimates of speeds of dinosaurs. *Nature* 261, 129-130.
- Alcalá, L., Lockley, M.G., Cobos, A., Mampel, L., Royo-Torres, R., 2016. Evaluating the dinosaur track record: an integrative approach to understanding the regional and global distribution, scientific importance, preservation, and management of tracksites. In: Falkingham, P.L., Marty, D., Richter, A. (Eds.), *Dinosaur Tracks: the Next Steps*. Indiana University Press, Bloomington; Indianapolis, pp. 101-117, 2016.

- Bates, K.T., Manning, P.L., Vila, B., Hodgetts, D., 2008. Three-dimensional modelling and analysis of dinosaur trackways. *Palaeontology* 51, 999–1010.
- Bates, K.T., Falkingham, P.L., Hodgetts, D., Farlow, J.O., Breithaupt, B.H., O'Brien, M., Matthews, N., Sellers, W.L., Manning, P.L., 2009. Digital imaging and public engagement in palaeontology. *Geol. Today* 25, 134–139.
- Bates, K.T., Falkingham, P.L., Rarity, F., Hodgetts, D., Purslow, A., Manning, P.L., 2010. Application of high-resolution laser scanning and photogrammetric techniques to data acquisition, analysis and interpretation in palaeontology. *Int. Arch. Photogram. Rem. Sens. Spatial Inf. Sci.* 38, 68–73.
- Belvedere, M., 2008. Ichnological Researches on the Upper Jurassic Dinosaur Tracks in the Iouaridène Area (Demnat, Central High-Atlas, Morocco). Ph.D thesis, Degli Studi Di Padova University, p. 128.
- Bemis, S.P., Micklethwaite, S., Turner, D., James, M.R., Akciz, S., Thiele, S.T., Bangash, H.A., 2014. Ground-based and UAV-Based photogrammetry: a multi-scale, high-resolution mapping tool for structural geology and paleoseismology. *J. Struct. Geol.* 69, 163–178.
- Breithaupt, B.H., Matthews, N.A., 2001. Preserving paleontological resources using photogrammetry and geographic information systems. In: Harmon, D. (Ed.), *Crossing Boundaries in Park Management: Proceedings of the 11th Conference on Research and Resource Management in Parks and Public Lands*. The George Wright Society, Hancock, Michigan, pp. 62–70.
- Breithaupt, B.H., Southwell, E.H., Adams, T., Matthews, N.A., 2001. Innovative documentation methodologies in the study of the most extensive dinosaur tracksite in Wyoming. In: Santucci, V.L., McClelland, L. (Eds.), *Proceedings of the 6th Fossil Research Conference*. National Park Service D-2228. National Park Service. Geological Resources Division, Lakewood, Colorado, pp. 113–122.
- Breithaupt, B.H., Matthews, N.A., Noble, T.A., 2004. An integrated approach to three-dimensional data collection at dinosaur tracksites in the Rocky Mountain West. *Ichnos* 11 (1–2), 11–26.
- Cobos, A., Alcalá, L., 2017. Palaeontological heritage as a resource for promoting geotourism in the rural setting: el Castellar (Teruel, Spain). *Geohierarchie* 10, 405–414.
- Doneus, M., 2013. Openness as visualization technique for interpretative mapping of airborne Lidar derived digital terrain models. *Rem. Sens.* 5, 6427–6442.
- Dozier, J., Frew, J., 1990. Rapid calculation of terrain parameters for radiation modeling from digital elevation data. *IEEE Trans. Geosci. Rem. Sens.* 28, 963–969.
- Falkingham, P.L., Margetts, L., Smith, I.M., Manning, P.L., 2009. Reinterpretation of palmate and semi-palmate (webbed) fossil tracks; insights from finite element modelling. *Palaeogeogr. Palaeoclimatol. Palaeoecol.* 271, 69–76.
- Falkingham, P.L., 2012. Acquisition of high resolution three-dimensional models using free, open-source, photogrammetric software. *Palaeontol. Electron.* 15 (1), 15.
- Falkingham, P.L., 2016. Applying objective methods to subjective track outlines. In: Falkingham, P.L., Marty, D., Richter, A. (Eds.), *Dinosaur Tracks: the Next Steps*. Indiana University Press, Bloomington; Indianapolis, pp. 72–80, 2016.
- Falkingham, P.L., Gatesy, S.M., 2014. The birth of a dinosaur footprint: subsurface 3D motion reconstruction and discrete element simulation reveal track ontogeny. *Proc. Natl. Acad. Sci. Unit. States Am.* 111 (51), 18279–18284.
- Falkingham, P.L., Marty, D., Richter, A., 2016. *Dinosaur Tracks: the Next Step*. Indiana University Press, Bloomington; Indianapolis, p. 611.
- Falkingham, P.L., Bates, K.T., Avanzini, M., Bennett, M., Bordy, E.M., Breithaupt, B.H., Castanera, D., Citton, P., Diaz-Martinez, I., Farlow, J.O., Fiorillo, A.R., Gatesy, S.M., Getty, P., Hatala, K.G., Hornung, J.J., Hyatt, J.A., Klein, H., Lallensack, J.N., Martin, A.J., Marty, D., Matthews, N.A., Meyer, C.A., Milàn, J., Minter, N.J., Razzolini, N.L., Romilio, A., Salisbury, S.W., Sciscio, L., Tanaka, I., Wiseman, A.L.A., Xing, L.D., Belvedere, M., 2018. A standard protocol for documenting modern and fossil ichnological data. *Palaeontology* 61 (4), 469–480.
- Gand, F., Fara, E., Durllet, C., Moreau, J.D., Caravaca, G., André, D., Lefillatre, R., Passet, A., Wiénin, M., Gély, J.P., 2018. Les pistes d'archosaures : *Kayentapus ubacensis* nov. isp. (Theropodes) et crocodylomorphes du Bathonien des Grands-Causse (France). *Conséquence paléo-biologiques, environnementales et géographiques*. *Ann. Paleontol.* 104 (3), 183–216.
- Gillette, D.D., Lockley, M.G., 1989. *Dinosaur Tracks and Traces*. Cambridge Univ. Press, Cambridge, p. 454.
- Graversen, O., Milàn, J., Loope, D.B., 2007. Dinosaur tectonics: a structural analysis of theropod undertracks with a reconstruction of theropod walking dynamics. *J. Geol.* 115, 641–654.
- Hitchcock, E., 1838. Report on a Re-examination of the Economical Geology of Massachusetts. Dutton and Wentworth. State printers, p. 152.
- Hitchcock, E., 1848. An attempt to discriminate and describe the animals that made the fossil footmarks of the United States, and especially of New England. *Mem. Am. Acad. Arts Sci.* 3, 129–256.
- Hitchcock, E., 1858. *Ichnology of New England: A Report on the Sandstone of the Connecticut Valley Especially its Fossil Footmarks*, Made to the Government of the Commonwealth of Massachusetts. William White printer, p. 374.
- Imhof, E., 2007. *Cartographic Relief Presentation*. Environmental Systems Research Institute Inc., U. S., third ed. ESRI Press, Redlands, p. 434.
- Ishigaki, S., Fujisaki, T., 1989. Three-dimensional representation of *Eubrontes* by the method of moiré topography. In: Gillette, D.D., Lockley, M.G. (Eds.), *Dinosaur Tracks and Traces*. Cambridge University Press, Cambridge, UK, pp. 421–425.
- Kraus, K., de Gryter, Walter, 2007. *Photogrammetry Geometry from Images and Laserscans*. In: second ed., p. 459.
- Lallensack, J.N., Van Heteren, A.H., Wings, O., 2016. Geometric morphometric analysis of intratrackway variability: a case study on theropod and ornithomimid dinosaur trackways from Münchelhagen (Lower Cretaceous, Germany). *Peer J* 4, e2059.
- Laws, E., Scott, N., 2003. Developing new tourism services: dinosaurs, a new drive tourism resource for remote regions? *J. Vacat. Mark.* 9, 368–380.
- Lockley, M.G., Houck, K.J., Prince, N.K., 1986. North America's largest dinosaur trackway site: implications for Morrison Formation paleoecology. *Geol. Soc. Am. Bull.* 97 (10), 1163–1176.
- Lockley, M.G., 1991. *Tracking Dinosaurs: a New Look at an Ancient World*. Cambridge University Press., Cambridge, p. 238.
- Longley, P., 2005. *Geographic Information Systems and Science*. John Wiley and Sons, p. 560.
- López, J.A.B., Jiménez, G.A., Romero, M.S., García, E.A., Martín, S.F., Medina, A.L., Guerrero, J.A.E., 2016. 3D modelling in archaeology: the application of Structure from Motion methods to the study of the megalithic necropolis of Panoria (Granada, Spain). *J. Archaeol. Sci. Rep.* 10, 495–506.
- Magail, J., Monna, F., Esin, Y., Wilczek, J., Yeruul-Erdene, C., Gantulga, J.-O., 2017. Applications de la photogrammétrie à la documentation de l'art rupestre, des chantiers de fouilles du bâti – mission du Musée d'Anthropologie préhistorique de Monaco. *Musee Anthropol. Prehist. Monaco* 56, 69–92.
- Mallison, H., Wings, O., 2014. Photogrammetry in paleontology – a practical guide. *Journal of Paleontological Techniques* 12, 1–31.
- Mara, H., Krömker, S., Jakob, S., Breuckmann, B., 2010. GigaMesh and gilgamesh - 3D multiscale integral invariant coneiform character extraction. *Proc. VAST Int. Symposium on Virtual Reality, Archaeology and Cultural Heritage* 131–138.
- Masrouf, M., Pascual-Arribas, C., de Ducla, M., Hernández-Medrano, N., Pérez-Lorente, F., 2017a. Anza palaeoichnological site. Late Cretaceous. Morocco. Part I. The first African pterosaur trackway (manus only). *J. Afr. Earth Sci.* 134, 766–775.
- Masrouf, M., Lkebir, N., Pérez-Lorente, F., 2017b. Anza palaeoichnological site. Late Cretaceous. Morocco. Part II. Problems of large dinosaur trackways and the first African Macropodosaurus trackway. *J. Afr. Earth Sci.* 134, 776–793.
- Matthews, N.A., Breithaupt, B.H., 2001. Close-range photogrammetric experiments at dinosaur ridge. *Mt. Geol.* 38 (3), 147–153.
- Matthews, N.A., Breithaupt, B.H., Noble, T.A., Titus, A., Smith, J., 2005. A geospatial look at the morphological variation of tracks at the Twentymile Wash dinosaur tracksite, Grand Staircase-Escalante National Monument, Utah. *J. Vertebr. Paleontol.* 25, 90A.
- Matthews, N.A., Noble, T.A., Breithaupt, B.H., 2006. The application of photogrammetry, remote sensing and geographic information systems (GIS) to fossil resource management. *Bull. N. M. Mus. Nat. Hist. Sci.* 34, 119–131.
- Matthews, N.A., Noble, T.A., Breithaupt, B.H., 2016. Close-range photogrammetry for 3-D ichnology: the basics of photogrammetric ichnology. In: Falkingham, P.L., Marty, D., Richter, A. (Eds.), *Dinosaur Tracks: the Next Steps*. Indiana University Press, Bloomington; Indianapolis, pp. 29–55, 2016.
- Mazin, J.M., Hantzpergue, P., Pouech, J., 2016. The dinosaur tracksite of loulle (early kimmeridgian; jura, France). *Geobios* 49 (3), 211–228.
- Milàn, J., Loope, D.B., 2007. Preservation and erosion of theropod tracks in eolian deposits: examples from the Middle Jurassic Entrada Sandstone, Utah. *U.S.A. J. Geol.* 115, 375–386.
- Monna, F., Esin, Y., Magail, J., Granjon, L., Navarro, N., Wilczek, J., Saligny, L., Couette, S., Dumontet, A., Chateau, C., 2018. Documenting carved stones by 3D modelling – example of Mongolian deer stones. *J. Cult. Herit.* 34, 116–128.
- Monbaron, M., Monbaron, J., 2015. La route des dinosaures : Itinéraires à travers le Geoparc M'Goun, Haut Atlas, Maroc. Région Tadmra-Azilal, p. 142.
- Moratalla, J.J., Sanz, J.L., Jimenez, S., 1988. Multivariate analysis on Lower Cretaceous dinosaur footprints: discrimination between ornithomimids and theropods. *Geobios* 21, 395–408.
- Moreau, J.-D., Trincal, V., Fara, E., Baret, L., Jacquet, A., Barbini, C., Flament, R., Wiénin, M., Bourel, B., Jean, A., 2020. Middle Jurassic tracks of sauropod dinosaurs in a deep karst cave from France. *J. Vertebr. Paleontol.* <https://doi.org/10.1080/02724634.2019.1728286>.
- Olivero, E.B., Ponce, J.J., Marsicano, C.A., Martinioni, D.R., 2007. Depositional settings of the basal lópez de Bertodano formation, maastrichtian, Antarctica. *Rev. Asoc. Geol. Argent.* 62, 521–529.
- Pérez-Lorente, F., 2015. *Dinosaur Footprints and Trackways of La Rioja Life of the Past*. Indiana University Press, p. 374.
- Reguero, M., Goin, F., Acosta Hospitaleche, C., Dutra, T., Marensi, S., 2013. Late Cretaceous/Paleogene West Antarctica terrestrial biota and its intercontinental affinities. *Springer Briefs in Earth System Sciences, South America and the Southern Hemisphere*, pp. 55–110.
- Remondino, F., Rizzi, A., Girardi, S., Massimo, P.F., Avanzini, M., 2010. 3D Ichnology—recovering digital 3D models of dinosaur footprints. *Photogramm. Rec.* 25 (131), 266–282.
- Reu, J.D., Plets, G., Verhoeven, G., Smedt, P.D., Bats, M., Cherretté, B., Maeyer, W.D., Deconynck, J., Herremans, D., Laloo, P., Meirvenne, M.V., Clercq, W.D., 2013. Towards a three-dimensional cost-effective registration of the archaeological heritage. *J. Archaeol. Sci.* 40, 1108–1121.
- Romilio, A., Salisbury, S.W., 2014. Large dinosaurian tracks from the Upper Cretaceous (Cenomanian–Turonian) portion of the Winton formation, Lark Quarry, central-western Queensland, Australia: 3D Photogrammetric analysis renders the 'stampe de trigger' scenario unlikely. *Cretac. Res.* 51, 186–207.
- Romilio, A., Hacker, J.M., Zlot, R., Poropat, G., Bosse, M., Steven, W.S., 2017. A multidisciplinary approach to digital mapping of dinosaurian tracksites in the lower cretaceous (Valanginian-Barremian) broome sandstone of the dampier peninsula, western Australia. *Peer J* <https://doi.org/10.7717/Peerj.3013>.
- Sarjeant, W.A.S., 1989. Ten paleoichnological commandments: a standardized procedure for the description of fossil vertebrate footprints. In: Gillette, D.D., Lockley, M.G. (Eds.), *Dinosaur Tracks and Traces*. Cambridge Univ. Press, Cambridge, p. 454.
- Tavani, S., Corradetti, A., Billi, A., 2016. High precision analysis of an embryonic extensional fault-related fold using 3D orthorectified virtual outcrops: the viewpoint importance in structural geology. *J. Struct. Geol.* 86, 200–210.

- Thulborn, T., 1990. Dinosaur Tracks. Chapman and Hall, p. 424.
- Verhoeven, G., Doneus, M., Briese, C., Vermeulen, F., 2012. Mapping by matching: a computer vision-based approach to fast and accurate georeferencing of archaeological aerial photographs. *J. Archaeol. Sci.* 39, 2060–2070.
- Westoby, M.J., Brasington, J., Glasser, N.F., Hambrey, M.J., Reynolds, J.M., 2012. 'Structure-from-Motion' photogrammetry: a low-cost, effective tool for geoscience applications. *Geomorphology* 179, 300–314.
- Wings, O., Lallensack, J.N., Mallison, H., 2016. The Early Cretaceous dinosaur trackways in MÜNCHENHAGEN (Lower Saxony, Germany): 3-D photogrammetry as basis for geometric morphometric analysis of shape variation and evaluation of material loss during excavation. In: Falkingham, P.L., Marty, D., Richter, A. (Eds.), *Dinosaur Tracks: the Next Steps*. Indiana University Press, Bloomington; Indianapolis, pp. 57–71, 2016.
- Yokoyama, R., Shirasawa, M., Pike, R.J., 2002. Visualizing topography by openness: a new application of image processing to digital elevation models. *Photogramm. Eng. Rem. Sens.* 68, 257–265.
- Zaksek, K., Ostir, K., Kokalj, Z., 2011. Sky-view factor as a relief visualization technique. *Rem. Sens.* 3, 398–415.